nature nanotechnology

Article

https://doi.org/10.1038/s41565-023-01406-2

Coherent magnon-induced domain-wall motion in a magnetic insulator channel

Received: 28 October 2022

Accepted: 23 April 2023

Published online: 01 June 2023



Check for updates

Yabin Fan © 1,4, Miela J. Gross © 2,4, Takian Fakhrul, Joseph Finley 2,3, Justin T. Hou^{2,3}, Steven Ngo¹, Lugiao Liu **©** ^{2,3} ⋈ & Caroline A. Ross **©** ¹ ⋈

Advancing the development of spin-wave devices requires high-quality low-damping magnetic materials where magnon spin currents can efficiently propagate and effectively interact with local magnetic textures. Here we show that magnetic domain walls can modulate spin-wave transport in perpendicularly magnetized channels of Bi-doped yttrium iron garnet. Conversely, we demonstrate that the magnon spin current can drive domain-wall motion in the Bi-doped yttrium iron garnet channel device by means of magnon spin-transfer torque. The domain wall can be reliably moved over 15-20 µm distances at zero applied magnetic field by a magnon spin current excited by a radio-frequency pulse as short as 1 ns. The required energy for driving the domain-wall motion is orders of magnitude smaller than those reported for metallic systems. These results facilitate low-switching-energy magnonic devices and circuits where magnetic domains can be efficiently reconfigured by magnon spin currents flowing within magnetic channels.

Spin waves, or magnons, can efficiently carry spin information over macroscopic distances in low-damping magnetic materials¹⁻⁴. Magnonic devices are free from certain drawbacks inherent to traditional electronics, such as dissipation of energy due to electric currents⁵⁻⁷, thus providing a promising platform for realizing ultralow-energy devices and circuits. More importantly, magnons can apply spin-transfer torque⁸⁻¹⁰ to a magnetic moment and enable useful functions such as magnetization reversal¹¹ or domain-wall (DW) motion^{12,13}. Conversely, magnetic textures such as DWs can attenuate and shift the phase of a magnon spin current¹³⁻¹⁶. Efficient mutual interactions between magnons and magnetic textures facilitate all-magnon spintronic devices, where magnons can be used to write magnetic bits through magnetization reversal or DW movement and read the bits via their effects on magnon propagation. In prior work, metallic Co/Ni multilayer films with perpendicular magnetic anisotropy (PMA) were utilized to study the interaction between coherent magnons and DWs¹³, but the large Gilbert damping ($\alpha = 0.024$) (ref. 13) and pinning of the DWs led to low DW velocity (~10 m s⁻¹) and high microwave power requirements. In contrast, low-damping magnetic insulators offer an improved materials platform for wave-based computing by reducing or eliminating dissipation and eddy currents and supporting fast switching dynamics.

In this work, we demonstrate mutual magnon-DW interactions in low-damping bismuth-doped yttrium iron garnet (Bi-YIG) ferrimagnetic films with PMA: the DW modifies the transmission of spin waves, and the spin waves drive DW depinning and long-range motion even for pulse lengths as low as 1 ns. As depicted by the schematic in Fig. 1a, spin waves and DWs interact via an exchange of angular momentum. Magnons on the left side of the DW carry spin $+\hbar$, whereas magnons on the right side carry spin $-\hbar$; when one magnon transits through the DW, a net spin angular momentum of $2\hbar$ is transferred into the DW, which is predicted to drive DW motion opposite to the direction of magnon flow^{8–10,17}. In this scenario, similar to current-driven DW motion below Walker breakdown¹⁸⁻²⁰, the DW velocity is predicted to linearly scale with the magnon spin current^{8,12,13}. In contrast, if magnons are reflected or absorbed by the DW, the exchange of linear momentum is predicted to drive the DW motion in the direction of the magnon flow, with dynamics that depend on the spin-wave frequency, amplitude and angle of incidence, as well as the type of DW and its own spectrum

Department of Materials Science and Engineering, Massachusetts Institute of Technology, Cambridge, MA, USA. Department of Electrical Engineering and Computer Science, Massachusetts Institute of Technology, Cambridge, MA, USA. 3Microsystems Technology Laboratories, Massachusetts Institute of Technology, Cambridge, MA, USA. 4These authors contributed equally: Yabin Fan, Miela J. Gross. 🖂 e-mail: luqiao@mit.edu; caross@mit.edu

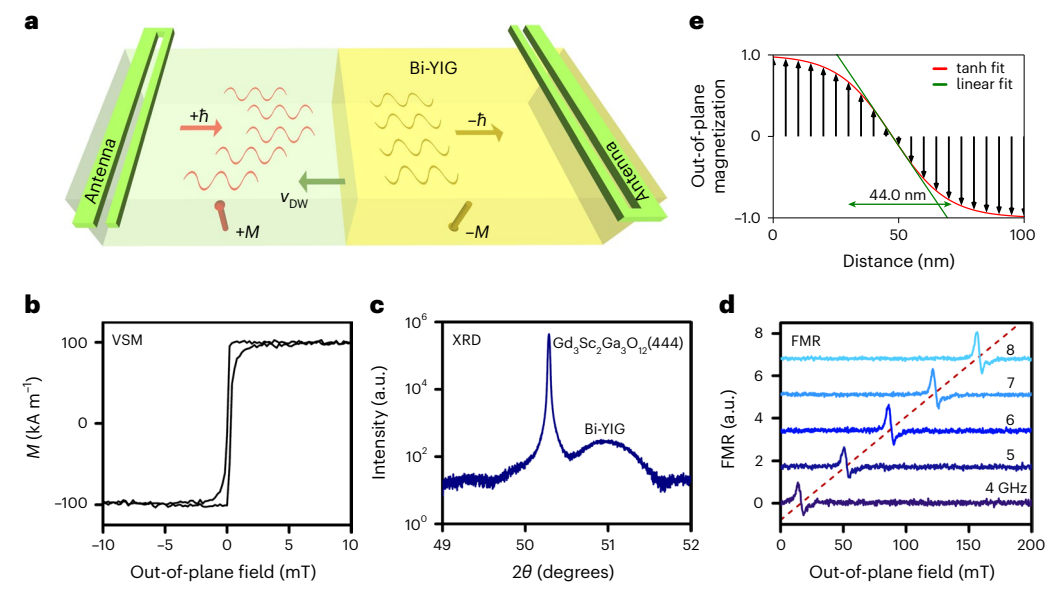


Fig. 1| **Schematic of magnon–DW mutual interaction and characterization of the Bi-YIG thin-film sample. a**, Illustration of magnons transmitting through a DW in Bi-YIG. The magnon on the left side of the DW carries spin $+\hbar$, whereas the magnon on the right side of the DW carries spin $-\hbar$; when a magnon travels through the DW, a net spin angular momentum of $2\hbar$ is transferred to the DW, leading to its motion with speed v_{DW} , **b**, Vibrating sample magnetometry (VSM)

measurement on the 17 nm Bi-YIG thin-film sample along the out-of-plane direction. **c**, X-ray diffraction (XRD) measurement on the Bi-YIG film. **d**, Field-differential FMR measurement on the Bi-YIG film sample under different frequencies, with the external field applied along the out-of-plane direction. **e**, Micromagnetic model of DW showing 44 nm width from a linear fit at the centre of the wall.

of excitations²¹⁻²⁷; interfacial symmetry breaking may also affect the spin-wave-driven DW propagation direction²⁸. There are few experimental demonstrations of spin-wave-driven or spin-wave-assisted DW $motion. \, Magnon\, currents\, originating\, from\, a\, temperature\, gradient\, via$ the spin Seebeck effect have been proposed to explain DW displacement in NiFe (ref. 29) and garnet films¹². Incoherent magnons generated by laser pulses³⁰ or DW collisions³¹ and coherent magnons from an antenna¹³ have been used to assist or drive DW motion in metallic films. There are also several examples of DWs modifying the transmission of spin waves in both metallic magnetic films^{13,14,16} and PMA garnet¹⁵, and DWs have been used as conduits, waveguides and magnonic crystals to filter or manipulate the propagation of spin waves 15,22,32-34. Unlike most prior experiments, the low-damping Bi-YIG material employed here enables the effective generation of coherent spin waves using a radio-frequency (RF) antenna at zero external magnetic field, and the magnon-driven DW motion induced by nanosecond RF pulses exhibits orders of magnitude lower energy consumption compared with that in metallic systems.

Results

The devices in this work were made from a 17-nm-thick Bi-YIG film grown on a Gd₃Sc₂Ga₃O₁₂(111) substrate using pulsed laser deposition (Methods)^{20,35,36}. Besides its low damping, Bi-YIG provides a high magneto-optical Kerr effect (MOKE), facilitating optical imaging of magnetic-domain. Vibrating sample magnetometry of the as-grown film (Fig. 1b) shows a square hysteresis loop along the out-of-plane direction, with a coercive field $\mu_0 H_c = 0.3$ mT and saturation magnetization of 100 kA m⁻¹. The PMA originates from both magnetostriction induced by epitaxial strain35 and growth-induced ordering of Bi and Y in the dodecahedral sites of the garnet³⁷. High-resolution X-ray diffraction measurements (Fig. 1c) indicate fully coherent film growth with high structural quality²⁰. Field-modulated ferromagnetic resonance (FMR) from 4 to 8 GHz was measured for fields along the out-of-plane direction (Fig. 1d). Zero-field FMR is realized at 3.5 GHz (Fig. 1d), which allows for the excitation of coherent magnons while maintaining a specific remanent DW configuration in the device. The Gilbert damping of similar 25-nm-thick samples measured in the 10–40 GHz range was as low as α = 1.3 × 10⁻⁴ with an inhomogeneous broadening linewidth of 2.7 mT (Supplementary Note 1), consistent with other measurements on Bi-YIG films ^{35,38}. This low damping greatly reduces the power dissipation during magnon excitation and propagation compared with metallic films ¹³.

The Bi-YIG film was patterned into racetrack structures with a width of 5 μm and length of 80 μm (Fig. 2, inset), surmounted by two Ti (10 nm)/Cu (100 nm)/Au (30 nm) microwave antennae for magnon excitation and detection 39,40 . The two antennae are U-shaped shorted coplanar waveguides (conductors are 1 and 2 μm wide, whereas the gap is 1 μm) 39 , placed 4 μm (Fig. 2, inset), 10 μm , 15 μm and 20 μm apart on the channel. The antenna design allows for the generation of coherent magnons over a range of gigahertz frequencies, differing from narrow-band magnons generated by d.c. spin injection 4,41 or non-coherent magnon excitation by a thermal gradient 12 or spin Hall effect 42 .

The propagation of magnons between the two antennae with and without the presence of a DW in the gap is studied by integrating the microwave circuits with a MOKE microscope¹³. In the setup (Fig. 2, inset), the magnon injector antenna was connected to a signal generator, whereas the detector antenna was connected to an RF diode detector. The transmission of magnons was measured using a field modulation technique by placing the modulation coil under the device chip (Supplementary Note 2). The magnetization state of the Bi-YIG channel was set by applying millisecond external magnetic-field pulses and was visualized from the MOKE contrast.

In Fig. 2, the transmitted microwave signal is plotted versus the microwave carrier frequency for remanent states without and with a DW between the two antennae. In the case without a DW, a maximum in the transmission was centred at 4.1 GHz, with a peak width of 0.3 GHz. The magnetic nature of the observed resonance can be confirmed by applying a d.c. external out-of-plane field $H_{\rm ext}$, which shifts the resonance frequency f (Supplementary Note 3). In the presence of a DW, a resonant signal was measured again at 4.1 GHz, with a width of 0.1 GHz (appearing at a negative voltage due to the reversal of magnetization).

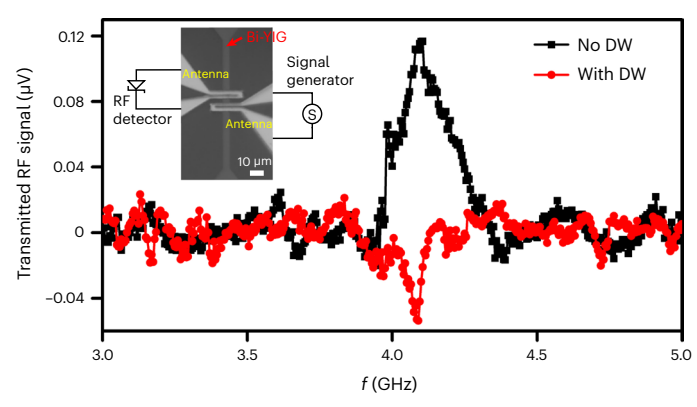
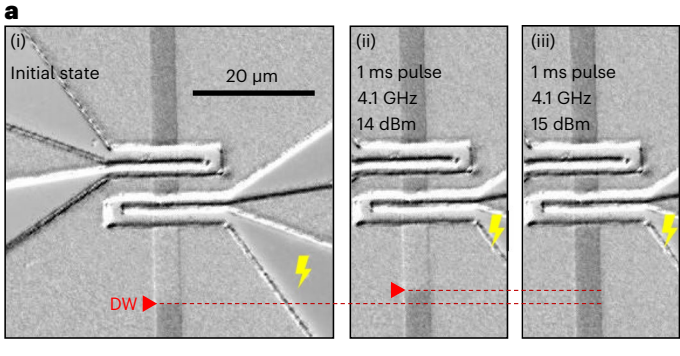


Fig. 2 | Magnon transmission spectrum on the Bi-YIG channel device with and without the presence of DW. Field-modulated magnon transmission spectrum measured for the device with uniform magnetization and with a DW in the gap between two antennae. The RF power used is 14 dBm. The inset shows the optical image of the 5- μ m-wide Bi-YIG channel device and an illustration of the instrument connection in the magnon transmission experiment. Two antennae, one injector and one detector are fabricated on top of the magnetic channel, separated by 4 μ m.

Comparing these two cases, we see that the resonance frequency is maintained but the signal amplitude is attenuated by a factor of 2.4 (or a power reduction by a factor of 5.8) after travelling through the DW. The attenuation in the transmitted magnon signal is consistent with previous results from a Co/Ni multilayer with PMA (ref. 13). An analysis of the magnon dispersion relation for the Bi-YIG shows that these magnons are exchange-mode spin waves 20,43 with a wavenumber of 67 μm^{-1} and a group velocity of 570 m s $^{-1}$, which leads to a propagation length on the order of tens of micrometres in the Bi-YIG channel (Supplementary Note 4).

To demonstrate magnon-induced DW motion, we first prepare a DW near one antenna by applying external magnetic-field pulses. In Fig. 3a(i), a DW (boundary between the grey and dark regions indicated with a red arrow) is formed close to the lower antenna. From micromagnetic modelling, the DW is of the Bloch type with a width of 44 nm (Fig. 1e and Supplementary Note 5). After the application of one RF microwave pulse of 14 dBm and 1 ms at 4.1 GHz onto the lower antenna. the DW moves by 3 µm towards the antenna: a second RF pulse of 15 dBm and 1 ms moves the DW all the way (by 12 µm) to the lower antenna edge. Here 4.1 GHz was chosen based on its high transmission amplitude (Fig. 2). In contrast, when the device was driven by off-resonance 2 GHz microwave pulses at the same power, no DW motion was detected (Supplementary Note 6). At 4.1 GHz, the DW moves towards the magnon source, which is consistent with the magnonic spin-transfer torque mechanism resulting from magnon transmission through the DW8-10,44, and different from both linear momentum transfer²¹ and field-induced DW movement in the presence of transient spin waves³¹ (in both these cases, the DWs move along the magnon propagation direction).

We then study the motion of the DW in the region of spin-wave channel between two antennae, reflecting a more practical configuration for programming the spin-wave conduit using magnon current. We note that DWs were commonly found near the edges of antennas, possibly because of local changes in anisotropy due to, for example, strain from the overlaid metal feature. Figure 3b(i) shows a device where the two antennae have a separation of $10~\mu m$. Here a DW was formed near the upper antenna edge with external magnetic-field pulses (indicated by the grey—white boundary and red arrow). By applying an RF pulse (2 dBm, 1 ms) at 4.1 GHz to the lower antenna, the DW moves by 2 μm towards the lower antenna (Fig. 3b(ii)). Subsequent pulses at 3 dBm and 1 ms and then at 4 dBm and 1 ms move the DW by 1 μm and then by 7 μm (Fig. 3b(iii)(iv)) towards the lower antenna. Therefore, the experiments



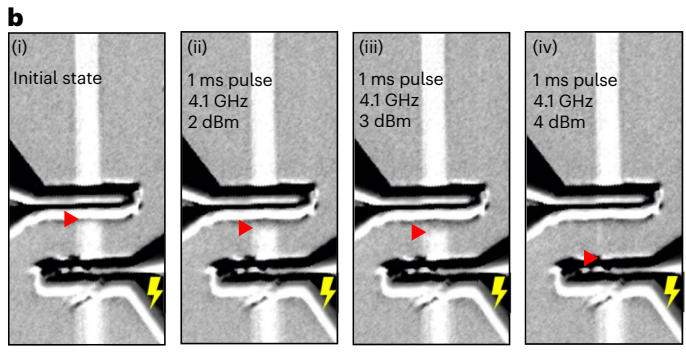


Fig. 3 | **Magnon-induced DW motion.** The injector antenna and DW are indicated with a yellow lightning bolt and red arrow, respectively. **a**, MOKE images of a DW in the initial state (i), after the first pulse at 14 dBm (ii) and the second pulse at 15 dBm (iii) applied at the lower antenna, using a 1 ms pulse at 4.1 GHz. In (iii), the DW moving towards the lower antenna probably annihilated with a DW pinned under that antenna. **b**, A DW formed near the upper antenna edge in the initial state (i) and after a 1 ms pulse at 2 dBm (iii), 3 dBm (iii) and 4 dBm (iv) applied at the lower antenna at 4.1 GHz.

in Fig. 3a,b demonstrate the progressive motion of the DW towards the source of spin waves. A local resistance measurement of the antenna (Fig. 4) and applying a 10 s 4.35 GHz pulse at 24 dBm showed a temperature increase of 0.07 K (Supplementary Note 7), which excludes possible Joule-heating-induced DW motion.

We explore the effects of incoming RF pulse power, width and frequency on DW motion in a third device with 15 µm separating the two antennae. We measured the RF power threshold required to initiate DW motion as a function of the carrier frequency of pulse and the pulse width. Figure 4a plots the power threshold as a function of carrier frequency for pulse widths of 1, 2, 3 and 75 ns. These data exhibit a minimum power threshold at 4.35 GHz for the device under test. A device with 10 µm separating the two antennae (Fig. 3b) gives similar conclusions but with a minimum power threshold at 4.1 GHz (Supplementary Note 8). The antenna design used here can produce an RF field over a range of frequencies, so the minimum power threshold is not attributed to the antenna geometry. Additional examples of spin-wave-driven DW motion are given in Supplementary Note 9, including a device that demonstrated DW motion of 20 µm. The frequency dependence of threshold power implies that the transfer of energy from the RF field into spin waves and/or the spin-wave-induced excitation, depinning and motion of the DW are most efficient at a particular frequency. Variability in the optimum frequency between devices probably reflects differences in their magnetic properties due to variations in deposition or patterning.

Figure 4a (inset) shows that an RF pulse as short as 1 ns (19 dBm) at 4.35 GHz caused the DW to move the entire 15 μm distance between the antennae. From the smallest measured power threshold for a 1 ns pulse width, we may estimate the energy required to translate a DW in the channel by estimating losses in the cables and connectors, the

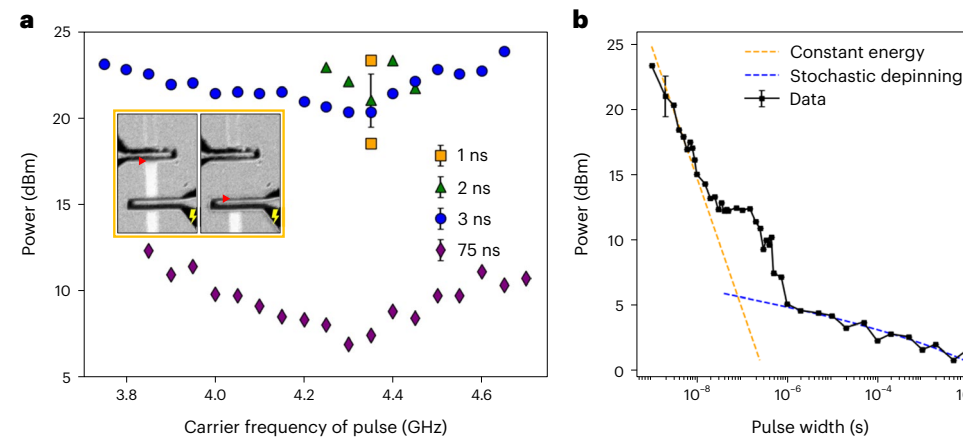


Fig. 4 | Magnon-induced DW motion power threshold dependence on pulse width and carrier frequency of pulse. a, Power threshold as a function of RF pulse frequency for pulse widths of 1, 2, 3 and 75 ns. An error bar is shown, based on the standard deviation of ten repeated measurements at one frequency. The inset shows the MOKE images of a 15- μm -gap device before and after the 1 ns 4.35 GHz pulse inducing DW motion at 19 dBm. b, DW motion power threshold

as a function of pulse width with a carrier frequency of 4.35 GHz. An error bar is shown, based on the standard deviation of ten repeated measurements at one pulse width. The orange dashed line shows the linear slope corresponding to a constant pulse energy. The blue dashed line corresponds to stochastic depinning fit for a pulse width of $\geq 1 \,\mu s$.

10

10

inefficiency of energy conversion from the RF signal into spin waves and the spin-wave energy dissipated by damping (Supplementary Note 10), yielding an order of magnitude estimate that the upper bound of energy used to propagate the DW by 15 µm is ≈4 pJ. This energy is orders of magnitude lower than the one reported in the Co/Ni metallic structure (energy to drive DW motion is almost of the order of microjoules), probably due to the low-damping, low-pinning and low-dissipation properties of the insulating Bi-YIG material.

We now consider the effect of pulse width on the power threshold at the optimum carrier frequency of 4.35 GHz for the device with 15 µm antenna separation (Fig. 4b). Here the power threshold generally increases when the pulse time is reduced. In the short-pulse regime (<0.1 μs), the slope of threshold power versus pulse width fits well to a model of constant energy (orange dashed line). In this regime, the energy transferred from the spin wave to the DW both depins and propagates the DW. Recalling that spin wave at frequency ω has a power $\omega \hbar n v_{sw} A$, where n, v_{sw} and A are the density and velocity of the magnons and the spin-wave channel cross-section area, respectively. A constant energy, therefore, indicates that the total number of transferred magnons within the pulse duration Δt , $nv_{sw}A\Delta t$, is a constant, consistent with the constant total angular momentum requirement for domain switching. For longer pulses ($\geq 1 \mu s$), the threshold power slowly decreases with increasing pulse length. We attribute the behaviour in the long-pulse regime to stochastic depinning of the DW at room temperature, in which spin-wave excitation of the DW is considered to lower the energy barrier for depinning through the magnonic spin torque. If we fit this regime using an Arrhenius law⁴⁵ (Supplementary Note 11), we find the energy barrier that pins the DW to be (0.62 ± 0.01) eV. This may be compared with values of 1.379 and 1.700 eV obtained in permalloy nanowires and 1.440 eV for FePt (refs. 45,46). The low magnetization, coercivity and damping of Bi-YIG may account for its lower pinning energy barrier compared with these metals.

Conclusions

In this work, we have demonstrated mutual interactions between magnons and DWs in channel devices made of low-damping, insulating and PMA thin-film material, namely, Bi-YIG. We show that the DW attenuates magnon transport. More importantly, we have shown that a magnon spin current generated by an RF pulse can reliably drive DW motion in a channel device, with a displacement of up to 15 µm resulting from a 1 ns pulse. The motion of the DW towards the source of spin waves indicates

that the transfer of angular momentum to the DW from transmitted spin waves dominates the spin wave-DW interaction, even though there is also the absorption or reflection of spin waves. The low Gilbert damping coefficient of Bi-YIG allows for long magnon decay lengths and the insulating properties of Bi-YIG further reduce Joule heating or conduction-electron-related dissipation, making this material ideal for low-energy wave-based computing. Unlike spin-orbit-torque-driven DW motion in Pt/Bi-YIG where an external in-plane field is needed to form a Néel-type DW²⁰, the magnon-driven DW motion does not require any specific type of DW and thus does not need the assistance of any external magnetic field 20,47. The Bi-YIG/Gd₃Sc₂Ga₃O₁₂ used here does not show measurable Dzyaloshinskii-Moriya interactions²⁰, so it does not support chiral textures. We anticipate that spin waves can also drive the motion of DWs and chiral textures in magnetic materials with sizable Dzyaloshinskii-Moriya interaction⁴⁸. To further reduce the power consumption, the antennas may be replaced by a more efficient magnon generation process, for example, using d.c. spin-Hall-effect-induced auto-oscillations^{49,50}. The high DW velocity and low power consumption enabled by low-damping PMA Bi-YIG facilitates applications in magnon-based spintronic devices and circuits where DWs may be effectively written, reconfigured and detected by a magnon current.

Online content

Any methods, additional references, Nature Portfolio reporting summaries, source data, extended data, supplementary information, acknowledgements, peer review information; details of author contributions and competing interests; and statements of data and code availability are available at https://doi.org/10.1038/s41565-023-01406-2.

References

- 1. Kruglyak, V. V., Demokritov, S. O. & Grundler, D. Magnonics. J. Phys. D. 43, 264001 (2010).
- 2. Serga, A. A., Chumak, A. V. & Hillebrands, B. YIG magnonics. J. Phys. D 43, 264002 (2010).
- 3. Khitun, A., Bao, M. & Wang, K. L. Magnonic logic circuits. J. Phys. D 43, 264005 (2010).
- 4. Kajiwara, Y. et al. Transmission of electrical signals by spinwave interconversion in a magnetic insulator. Nature 464, 262-266 (2010).
- Chumak, A. V., Vasyuchka, V. I., Serga, A. A. & Hillebrands, B. Magnon spintronics. Nat. Phys. 11, 453-461 (2015).

- Csaba, G., Papp, Á. & Porod, W. Perspectives of using spin waves for computing and signal processing. *Phys. Lett. A* 381, 1471–1476 (2017).
- Sheng, L., Chen, J., Wang, H. & Yu, H. Magnonics based on thin-film iron garnets. J. Phys. Soc. Jpn 90, 081005 (2021).
- Yan, P., Wang, X. S. & Wang, X. R. All-magnonic spin-transfer torque and domain wall propagation. *Phys. Rev. Lett.* 107, 177207 (2011).
- Kovalev, A. A. & Tserkovnyak, Y. Thermomagnonic spin transfer and Peltier effects in insulating magnets. *Europhys. Lett.* 97, 67002 (2012).
- Hinzke, D. & Nowak, U. Domain wall motion by the magnonic spin Seebeck effect. *Phys. Rev. Lett.* 107, 027205 (2011).
- Wang, Y. et al. Magnetization switching by magnon-mediated spin torque through an antiferromagnetic insulator. Science 366, 1125–1128 (2019).
- Jiang, W. et al. Direct imaging of thermally driven domain wall motion in magnetic insulators. Phys. Rev. Lett. 110, 177202 (2013).
- 13. Han, J., Zhang, P., Hou, J. T., Siddiqui, S. A. & Liu, L. Mutual control of coherent spin waves and magnetic domain walls in a magnonic device. *Science* **366**, 1121–1125 (2019).
- Pirro, P. et al. Experimental observation of the interaction of propagating spin waves with Néel domain walls in a Landau domain structure. Appl. Phys. Lett. 106, 232405 (2015).
- Sheng, L. et al. Spin wave propagation in a ferrimagnetic thin film with perpendicular magnetic anisotropy. Appl. Phys. Lett. 117, 232407 (2020).
- Wojewoda, O. et al. Propagation of spin waves through a Néel domain wall. Appl. Phys. Lett. 117, 022405 (2020).
- Mikhailov, A. V. & Yaremchuk, A. I. Forced motion of a domain wall in the field of a spin wave. *JETP Lett.* 39, 354–357 (1984).
- Kishine, J.-I. & Ovchinnikov, A. S. Adiabatic and nonadiabatic spin-transfer torques in the current-driven magnetic domain wall motion. *Phys. Rev. B* 81, 134405 (2010).
- 19. Burrowes, C. et al. Non-adiabatic spin-torques in narrow magnetic domain walls. *Nat. Phys.* **6**, 17–21 (2010).
- Caretta, L. et al. Relativistic kinematics of a magnetic soliton. Science 370, 1438–1442 (2020).
- Wang, X.-G., Guo, G.-H., Nie, Y.-Z., Zhang, G.-F. & Li, Z.-X. Domain wall motion induced by the magnonic spin current. *Phys. Rev. B* 86, 054445 (2012).
- 22. Chang, L.-J. et al. Ferromagnetic domain walls as spin wave filters and the interplay between domain walls and spin waves. *Sci. Rep.* **8**, 3910 (2018).
- 23. Wang, X.-G., Guo, G.-H., Zhang, G.-F., Nie, Y.-Z. & Xia, Q.-L. Spin-wave resonance reflection and spin-wave induced domain wall displacement. *J. Appl. Phys.* **113**, 213904 (2013).
- 24. Han, D.-S. et al. Magnetic domain-wall motion by propagating spin waves. *Appl. Phys. Lett.* **94**, 112502 (2009).
- Seo, S.-M., Lee, H.-W., Kohno, H. & Lee, K.-J. Magnetic vortex wall motion driven by spin waves. Appl. Phys. Lett. 98, 012514 (2011).
- 26. Kim, J. S. et al. Interaction between propagating spin waves and domain walls on a ferromagnetic nanowire. *Phys. Rev. B* **85**, 174428 (2012).
- Risinggård, V., Tveten, E. G., Brataas, A. & Linder, J. Equations of motion and frequency dependence of magnon-induced domain wall motion. *Phys. Rev. B* 96, 174441 (2017).
- 28. Kim, K.-W. et al. Unidirectional magnon-driven domain wall motion due to the interfacial Dzyaloshinskii-Moriya interaction. *Phys. Rev. Lett.* **122**, 147202 (2019).
- Torrejon, J. et al. Unidirectional thermal effects in current-induced domain wall motion. *Phys. Rev. Lett.* **109**, 106601 (2012).
- Shokr, Y. A. et al. Steering of magnetic domain walls by single ultrashort laser pulses. *Phys. Rev. B* 99, 214404 (2019).
- Woo, S., Delaney, T. & Beach, G. S. D. Magnetic domain wall depinning assisted by spin wave bursts. *Nat. Phys.* 13, 448–454 (2017).

- 32. Hämäläinen, S. J., Madami, M., Qin, H., Gubbiotti, G. & van Dijken, S. Control of spin-wave transmission by a programmable domain wall. *Nat. Commun.* **9**, 4853 (2018).
- Banerjee, C. et al. Magnonic band structure in a Co/Pd stripe domain system investigated by Brillouin light scattering and micromagnetic simulations. *Phys. Rev. B* 96, 024421 (2017).
- Liu, C. et al. Current-controlled propagation of spin waves in antiparallel, coupled domains. *Nat. Nanotechnol.* 14, 691–697 (2019).
- 35. Soumah, L. et al. Ultra-low damping insulating magnetic thin films get perpendicular. *Nat. Commun.* **9**, 3355 (2018).
- Fakhrul, T. et al. Magneto-optical Bi:YIG films with high figure of merit for nonreciprocal photonics. Adv. Opt. Mater. 7, 1900056 (2019).
- 37. Callen, H. On growth-induced anisotropy in garnet crystals. *Mater. Res. Bull.* **6**, 931–938 (1971).
- 38. Kumar, R., Samantaray, B. & Hossain, Z. Ferromagnetic resonance studies of strain tuned Bi:YIG films. *J. Phys. Condens. Matter* **31**, 435802 (2019).
- Bailleul, M., Olligs, D., Fermon, C. & Demokritov, S. O. J. E. L. Spin waves propagation and confinement in conducting films at the micrometer scale. *Europhys. Lett.* 56, 741–747 (2001).
- Vlaminck, V. & Bailleul, M. Spin-wave transduction at the submicrometer scale: experiment and modeling. *Phys. Rev. B* 81, 014425 (2010).
- 41. Collet, M. et al. Generation of coherent spin-wave modes in yttrium iron garnet microdiscs by spin-orbit torque. *Nat. Commun.* **7**, 10377 (2016).
- Cornelissen, L. J., Liu, J., Duine, R. A., Youssef, J. B. & van Wees, B. J. Long-distance transport of magnon spin information in a magnetic insulator at room temperature. *Nat. Phys.* 11, 1022–1026 (2015).
- Oh, S.-H. et al. Coherent terahertz spin-wave emission associated with ferrimagnetic domain wall dynamics. *Phys. Rev. B* 96, 100407 (2017).
- 44. Cheng, Y., Chen, K. & Zhang, S. Giant magneto-spin-Seebeck effect and magnon transfer torques in insulating spin valves. *Appl. Phys. Lett.* **112**, 052405 (2018).
- 45. Wuth, C., Lendecke, P. & Meier, G. Temperature-dependent dynamics of stochastic domain-wall depinning in nanowires. *J. Phys. Condens. Matter* **24**, 024207 (2012).
- 46. Nguyen, V. D. et al. Elementary depinning processes of magnetic domain walls under fields and currents. Sci. Rep. 4, 6509 (2014).
- 47. Avci, C. O. et al. Interface-driven chiral magnetism and current-driven domain walls in insulating magnetic garnets. *Nat. Nanotechnol.* **14**, 561–566 (2019).
- Caretta, L. et al. Interfacial Dzyaloshinskii-Moriya interaction arising from rare-earth orbital magnetism in insulating magnetic oxides. Nat. Commun. 11, 1090 (2020).
- 49. Duan, Z. et al. Nanowire spin torque oscillator driven by spin orbit torques. *Nat. Commun.* **5**, 5616 (2014).
- 50. Demidov, V. E. et al. Magnetic nano-oscillator driven by pure spin current. *Nat. Mater.* **11**, 1028–1031 (2012).

Publisher's note Springer Nature remains neutral with regard to jurisdictional claims in published maps and institutional affiliations.

Springer Nature or its licensor (e.g. a society or other partner) holds exclusive rights to this article under a publishing agreement with the author(s) or other rightsholder(s); author self-archiving of the accepted manuscript version of this article is solely governed by the terms of such publishing agreement and applicable law.

© The Author(s), under exclusive licence to Springer Nature Limited 2023

Methods

Material growth

Here 17 nm Bi-YIG was grown by pulsed laser deposition at 560 °C substrate temperature and 150 mtorr oxygen pressure from a Bi_{0.8}Y_{2.2}Fe₅O₁₂ target onto a Gd₃Sc₂Ga₃O₁₂(111) substrate^{20,36}. The 248 nm KrF COMPex excimer laser was operated at 400 mJ per pulse (fluence, ~1.9 J cm⁻²), 10 Hz laser repetition rate and 6 cm target–substrate distance. The chamber was pumped to 6×10^{-6} torr before introducing oxygen. The films were cooled to room temperature at 10 °C min⁻¹ in 230 torr oxygen.

Integrated microwave and MOKE setup

The device was attached onto a coplanar waveguide printed circuit board (PCB) with a central hollow area. The PCB had two RF connectors on the two ends. The antennae on the device were connected to the signal line and ground on each side of the PCB waveguide using wire bonding. The PCB was mounted onto a circular modulation coil and the assembly was installed onto a MOKE microscope stage. The modulation coil could provide a field of about 0.2 mT, well below the channel coercivity of 15.0 mT, and the modulation frequency is 100 Hz. Another perpendicular electromagnet was installed on the MOKE microscope from underneath and its pole was extended through the modulation coil to approach the underside of the PCB. This perpendicular electromagnet applied a d.c. magnetic field to the device to initialize the domain configuration. The two RF connectors on the PCB were connected to the RF signal generator or RF diode by coaxial cables for the microwave experiment. Supplementary Note 2 provides more details of the integrated microwave and MOKE setup.

Microwave pulse experiment

To generate microwave pulses with width longer than 50 ns, we utilized the intrinsic pulse generation function within the Anritsu 68369A/NV synthesized signal generator. For microwave pulses shorter than 25 ns, we combined the Anritsu signal generator with an arbitrary pulse generator (Hewlett Packard 8131A) through a multiplexer to multiply the nanosecond pulse function (from the arbitrary pulse generator) with the microwave signal (from the Anritsu signal generator) and characterized the microwave pulse profile using an oscilloscope. The microwave pulse magnitude generated in both cases was calibrated by an Anritsu spectrum analyser, and the loss from both setups was calibrated by a vector network analyser.

Data availability

The data that support the findings of this study are available from the corresponding authors upon reasonable request.

Acknowledgements

C.A.R., M.J.G., Y.F. and T.F. acknowledge support from SMART, one of seven centres of nCORE, a Semiconductor Research Corporation program, sponsored by the National Institute of Standards and Technology (NIST), and the National Science Foundation under award DMR 1808190. S.N. was supported by Fujikura. L.L. acknowledges financial support from the National Science Foundation under award DMR-2104912. Shared facilities of CMSE (MRSEC DMR-1419807) were used. We thank S.-K. Kim for helpful discussions on spin wave dispersion in the Bi-YIG material.

Author contributions

T.F. grew the Bi-YIG material and performed the X-ray diffraction characterization. J.F. fabricated the devices and measured the vibrating sample magnetometry data. Y.F. carried out the microwave FMR and spin-wave transmission experiments. Y.F. and M.J.G. carried out the spin-wave-induced DW motion experiment. J.T.H. performed the wire bonding and helped with the microwave experiments. S.N. performed the micromagnetic modelling. C.A.R. and L.L. guided the research. Y.F., M.J.G. and C.A.R. wrote the paper with input from all the co-authors.

Competing interests

The authors declare no competing interests.

Additional information

Supplementary information The online version contains supplementary material available at https://doi.org/10.1038/s41565-023-01406-2.

Correspondence and requests for materials should be addressed to Lugiao Liu or Caroline A. Ross.

Peer review information *Nature Nanotechnology* thanks Philipp Pirro and Morgan Trassin for their contribution to the peer review of this work.

Reprints and permissions information is available at www.nature.com/reprints.